Title	Artificial Topological Superconductor by the Proximity Effect
Author(s)	Xu, JP; Liu, CH; Wang, MX; Ge, JF; Liu, ZL; Yang, XJ; Chen, Y; Liu, Y; Xu, ZA; Gao, CL; Qian, D; Zhang, F; Jia, JF
Citation	Physical Review Letters, 2014, v. 112 n. 21, article no. 217001, p. 217001:1-5
Issued Date	2014
URL	http://hdl.handle.net/10722/203328
Rights	Physical Review Letters. Copyright © American Physical Society.

Artificial Topological Superconductor by the Proximity Effect

Jin-Peng Xu,[1] Canhua Liu,[1] Mei-Xiao Wang,[1] Jianfeng Ge,[1] Zhi-Long Liu,[1] Xiaojun Yang,[2] Yan Chen,[3] Ying Liu,[1,4] Zhu-An Xu,[2] Chun-Lei Gao,[1] Dong Qian,[1] Fu-Chun Zhang,[2,5] and Jin-Feng Jia[1,*]

[1]*Key Laboratory of Artificial Structures and Quantum Control (Ministry of Education), Department of Physics and Astronomy, Shanghai Jiao Tong University, Shanghai 200240, China*

[2]*State Key Laboratory of Silicon Materials and Department of Physics, Zhejiang University, Hangzhou 310027, China*

[3]*Department of Physics, Fudan University, Shanghai 200433, China*

[4]*Department of Physics and Materials Research Institute, Pennsylvania State University, University Park, Pennsylvania 16802, USA*

[5]*Department of Physics, Hong Kong University, Hong Kong, China*

(Received 25 February 2014; published 30 May 2014)

Topological superconductors (TSCs), featuring fully gapped bulk and gapless surface states as well as Majorana fermions, have potential applications in fault-tolerant topological quantum computing. Because TSCs are very rare in nature, an alternative way to study the TSC is to artificially introduce superconductivity into the surface states of a topological insulator through the proximity effect [X. L. Qi, T. L. Hughse, S. Raghu, and S. C. Zhang, Phys. Rev. Lett. 102, 187001 (2009); L. Fu and C. L. Kane, Phys. Rev. Lett. 100, 096407 (2008); J. Alicea, Rep. Prog. Phys. 75, 076501 (2012); C. W. J. Beenakker, Annu. Rev. Condens. Matter Phys. 4, 113 (2013)]. Here we report the experimental realization of the proximity effect–induced TSC in Bi_2Te_3 thin films grown on a $NbSe_2$ substrate, as demonstrated by the density of states probed using scanning tunneling spectroscopy. We observed Abrikosov vortices and Andreev lower energy bound states on the surface of the topological insulator, with the superconducting coherence length depending on the film thickness and the magnetic field. These results also indicate that the topological surface states of Bi_2Te_3 thin films are superconducting and, thus, that the $Bi_2Te_3/NbSe_2$ is an artificial TSC. The feasibility of fabricating a TSC with an individual Majorana fermion bound to a superconducting vortex for topological quantum computing is discussed.

DOI: 10.1103/PhysRevLett.112.217001 PACS number 74.45.+c, 03.65.Vf, 74.25.Ha, 74.55.+v

When a normal metal and a superconductor are brought into contact, Cooper pairs will be introduced into the normal metal through the interface, resulting in a superconducting energy gap on the Fermi level (E_F); this is known as the superconducting proximity effect [1]. The pairing symmetry of the proximity effect–induced Cooper pairs is determined by the electronic structures of the normal metal. Topological superconductors (TSCs) with a p-wave-like pairing state and time reversal symmetry are predicted to host Majorana fermions [2,3]. A semiconductor nanowire with strong spin-orbit coupling fabricated on an s-wave superconductor may also realize Majorana fermions located at the ends of the nanowire under a suitable magnetic field [4,5]. Another proposed construction of TSCs is a three-dimensional topological insulator (TI) that has a spin-textured topological surface state band located in the bulk energy gap [6,7]. Fu and Kane predicted that when Cooper pairs are introduced to its topological surface states via the proximity effect, the surface of the TI will turn into a TSC that can host Majorana fermions in Abrikosov vortex cores [8].

Recently, proximity effect–induced superconductivity in surface states of a TI has been found in electronic transport measurement of several heterostructures involving a TI and superconductor [9–13]. However, the pairing symmetry has not been determined. While an indirect signature of Majorana fermions was revealed in a Josephson current measurement performed on an $Al/Bi_2Se_3/Al$ junction [11], more explicit evidence for a TSC with Majorana fermions is yet to be obtained. Abrikosov vortices in ordinary type II superconductors are well known [14–16], but their existence in proximity-induced TSCs has not been demonstrated, mainly due to the difficulty in preparing an atomically smooth interface between a TI and a superconductor. We previously reported the preparation of heterostructures by growing a Bi_2Se_3 thin film on a $NbSe_2$ single crystal, where the coexistence of Cooper pairs and topological surface states was demonstrated [17].

Here we report the observation of proximity effect–induced superconductivity in a different heterostructure, $Bi_2Te_3/NbSe_2$, by scanning tunneling microscopy and spectroscopy (STM and STS). We systematically studied multiple quintuple layers (QL) of Bi_2Te_3 on top of $NbSe_2$. When the topological surface states form at 3QL, the superconducting tunneling spectra of the $Bi_2Te_3/NbSe_2$ surface appear to deviate from the usual s-wave spectra. We also observed Abrikosov vortices and bound states inside the vortex core, which should include the Majorana fermion predicted in theory at the zero bias. These experimental results provide the evidence for proximity-induced TSC

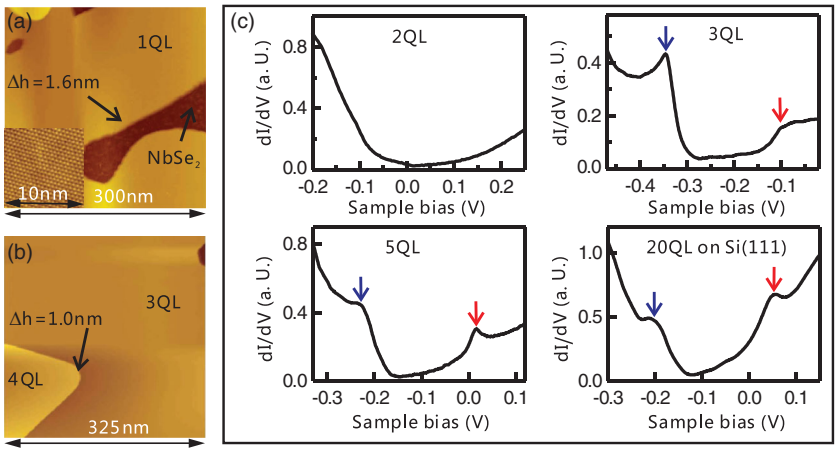

FIG. 1 (color). Morphology and electronic density of states of Bi_2Te_3 thin films of different coverages, grown on a $NbSe_2$ substrate. (a) and (b) Large-scale STM images of Bi_2Te_3 thin films. The inset in (a) shows the atomic resolution of the Bi_2Te_3 surface taken on a 3QL terrace. (c) dI/dV spectra measured at 4.2 K on 2QL, 3QL, and 5QL $Bi_2Te_3/NbSe_2$ heterostructures and on a 20QL Bi_2Te_3 film grown on a Si(111) surface. Blue and red arrows indicate the energy position of VBM and CBM, respectively.

states on the surface of a TI, paving the way for detecting Majorana fermions in the future.

All experiments were performed *in situ* on a commercial apparatus with base pressures of 3×10^{-10} torr for sample growth and 7×10^{-11} torr for STM measurement. $NbSe_2$ crystal was cleaved at room temperature in UHV after sufficient degassing at 250 °C. Te and Bi atoms were codeposited onto the $NbSe_2$ surface at 250 °C. Five minutes of post annealing was conducted to eliminate excess Te atoms in the Bi_2Te_3 films. All prepared samples were transferred to a cooling stage kept at 4.2 K for STM measurement, in which electrochemically etched tungsten tips were used after heating and silver decoration *in situ*. The *in situ* treatment of tungsten tips is to provide a nearly constant density of states (DOS) near E_F at the side of STM tip, so that the local DOS on the sample side can be correctly recorded in STS measurement. A lower sample temperature of 0.4 K was achieved by using liquid ^{3}He. To obtain dI/dV spectra at a given location, the tip-sample separation was held constant and a lock-in amplifier was used to modulate the bias voltage by dV (0.15 mV or 3 mV depending on the spectral range of interest) with a frequency of 991 Hz. The vortex image is the record of each pixel's zero-bias conductance (ZBC), while the bias voltage is ramped from 5 mV to 0 V with feedback off.

The growth mode of Bi_2Te_3 is the same as that of Bi_2Se_3 on $NbSe_2$ [17], i.e., layer-by-layer growth as shown in Figs. 1(a)–1(b). The excellent crystallization of the Bi_2Te_3 film is seen in its STM image with an atomic resolution. Because of its higher growth temperature, the Bi_2Te_3 film has very large terraces, which are crucial for observing vortices in this work. The Bi_2Te_3 film is not interfaced with the $NbSe_2$ substrate directly; it is separated by a Bi layer in between, so that the first QL of Bi_2Te_3 has a step height of 1.6 nm in STM images. All other QLs have the thickness of 1.0 nm, similar to those grown on a Si(111) substrate [18]. Previous studies found that the topological surface state of a Bi_2Te_3 thin film grown on Si(111) does not form a Dirac cone until the thickness reaches 2QL to 4QL; this is because of the hybridization between the top and bottom surface states of the film [19–21]. Once the Dirac cone forms, the band structure near the Fermi energy does not change dramatically, except for a rigid energy shift with the increasing thickness of the Bi_2Te_3 film. On the $NbSe_2$ substrate, we observed a similar evolution of the electronic states in STS data with the increase of Bi_2Te_3 thickness, as shown in Fig. 1(c). The differential conductance curve (dI/dV spectrum) taken with STS, obtained on a 20QL Bi_2Te_3 film grown on a Si(111) surface, has a deformed U-shape segment in the energy range between the bulk valence band maximum (VBM) and the conduction band minimum (CBM), as indicated by blue and red arrows in Fig. 1(c), respectively. Similar deformed U-shape segments are also seen in dI/dV spectra taken on $Bi_2Te_3/NbSe_2$ at thicknesses of no less than 3QL. With the increase of Bi_2Te_3 thickness, the deformed U-shape segment shifts to a higher binding energy while keeping its size in the energy scale. This indicates that the topological surface states on $Bi_2Te_3/NbSe_2$ come into existence at a thickness of 3QL, which is a very similar behavior to that of Bi_2Te_3 films grown on Si(111) substrates [19]. We can also see that the Fermi level moves down with increasing film thickness; it is almost in the bulk band gap in 5QL films.

The superconducting energy gap was observed on the Bi_2Te_3 thin films in STS data. Figure 2(a) is a series of dI/dV spectra taken on $Bi_2Te_3/NbSe_2$ at 0.4 K; it shows strong thickness dependence. Figure 2(b) presents the dI/dV spectra of bare $NbSe_2$, 2QL, and 3QL Bi_2Te_3 films. Up to a thickness of 2QL, the STS curve has a flat bottom that touches the zero value of the differential conductance at around zero bias. The STS curve can be well fitted by an s-wave BCS-type spectrum function [Fig. 2(b), bottom and middle]. In contrast, the spectra of Bi_2Te_3 films of more than 2QL have nonflat bottoms that do not touch the zero of the differential conductance. Clearly, an s-wave BCS-type spectral function can no longer fit the spectrum of a 3QL Bi_2Te_3 film [Fig. 2(b), top]. A simple s-wave BCS tunneling spectrum cannot reproduce the spectrum near zero bias and the sharp coherence peak near the position of the energy gap, which

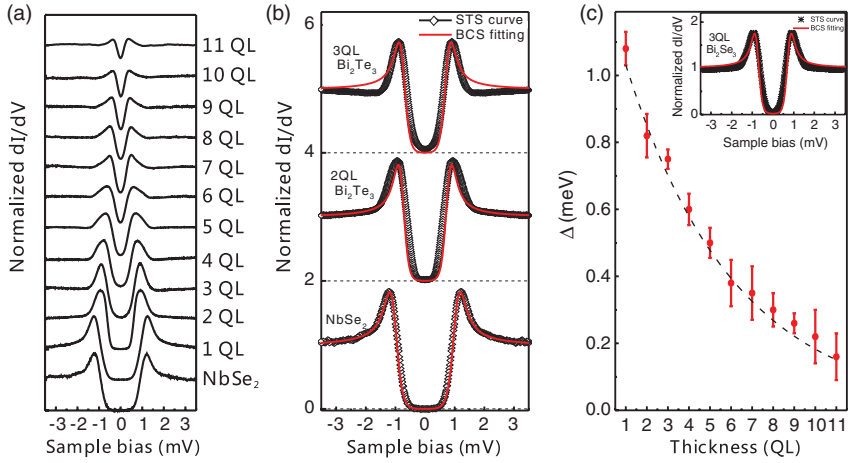

FIG. 2 (color). Superconducting energy gap observed on $Bi_2Te_3/NbSe_2$. (a) A series of dI/dV spectra taken on different thicknesses of Bi_2Te_3 thin films at 0.4 K. (b) dI/dV spectra measured at 0.4 K of bare $NbSe_2$, as well as 2QL and 3QL of Bi_2Te_3 thin films. All spectra are superimposed with standard BCS-like fitting results. The latter two spectra are shifted upward by 2 and 4, respectively. (c) Thickness dependence of the energy gap obtained from the BCS-like fitting. The dashed line indicates an exponential decay of the gap. The dI/dV spectra measured at 0.4 K on 3QL of a Bi_2Se_3 thin film on $NbSe_2$ superimposed with standard BCS-like fitting result is shown in the inset.

could be due to weakened superconductivity through the TI film or an increased quasiparticle lifetime. Such behavior was not observed on 1QL or 2QL films. As the film increases in thickness, an abrupt change was seen on 3QL films, where TI surface states start to form. The formation of TI surface states could play an important role in the observed deviation of the dI/dV spectrum from s-wave BCS behavior in the 3QL structure [22,23]. To confirm this, the dI/dV spectrum taken on 3QL $Bi_2Se_3/NbSe_2$ at 0.4 K is also compared with a standard BCS tunneling spectrum [Fig. 2(c), inset]; we can see the agreement is much better than on 3QL Bi_2Te_3 film.

The data up to 11QL are fitted by thermally broadened s-wave BCS-like curves [24], and the results are summarized in Fig. 2(c). Roughly speaking, the gap value decreases exponentially as the thickness increases; this is qualitatively consistent with the energy gap decay for proximity effect–induced superconductivity.

Because the formation of the small energy gap at the Fermi level is due to quasiparticle excitations in a superconductor, the dI/dV spectra measured on $Bi_2Te_3/NbSe_2$ should also have strong dependence on external magnetic fields, which suppress the formation of Cooper pairs. In Fig. 3(a), we show a series of spatially averaged dI/dV spectra taken on a 3QL $Bi_2Te_3/NbSe_2$ sample at various perpendicular magnetic fields. With the increase of the magnetic field, the energy gap becomes smaller and the gap feature near the zero bias in the dI/dV spectra becomes shallower. The energy gap disappears at about 2.4 T, which is substantially smaller than the upper (perpendicular) critical field H_{c2} (3.2 T) of the $NbSe_2$ substrate.

Large terraces of the $Bi_2Te_3/NbSe_2$ surface make it possible to image Abrikosov vortices with STS [25]. Figures 3(b)–3(c) show dI/dV maps at zero bias, i.e., the contour of ZBC, recorded on a 3QL $Bi_2Te_3/NbSe_2$ and bare $NbSe_2$ surfaces under perpendicular magnetic fields. It is seen from Fig. 3(c) that the vortices exhibit a highly ordered hexagonal lattice, just like those observed on the clean $NbSe_2$ surface shown in Fig. 3(b). Because of the crystalline band structure and the interaction of the neighboring vortices in the hexagonal lattice, a sixfold symmetry is explicitly observed in the vortex images of the bare $NbSe_2$ surface [Fig. 3(d)]. The same symmetry is also present on the ZBC contour of the 5QL Bi_2Te_3 film [Fig. 3(e)]. The growth of Bi_2Te_3 films on $NbSe_2$ does not change the orientation of the vortex lattice; this is to avoid extra energy consumption for a magnetic flux penetrating the $Bi_2Te_3/NbSe_2$ samples. This may be seen with the aid of the two hexagons superimposed on Figs. 3(d) and 3(e) (dashed lines). Also, from the size of the unit cell of the vortex lattice, we can calculate the magnetic flux penetrating through one vortex cylinder. The obtained value is very close to a magnetic flux quantum, i.e., $\Phi_0 = h/2e$, in which h is Planck's constant and e is the electric charge of an electron.

By carefully comparing the vortices obtained on $NbSe_2$ and 3QL Bi_2Te_3, shown in Figs. 3(b) and 3(c), respectively, one can see that the vortex size is a little smaller on $NbSe_2$ than on 3QL Bi_2Te_3. We investigated the spatial extension of the vortex for different Bi_2Te_3 thicknesses. The ZBC line profile crossing through the center of the vortex can be very well fitted by the formula below, derived from the Ginzburg-Landau (GL) expression for the superconducting order parameter [16],

$$\sigma(r,0) = \sigma_0 + (1-\sigma_0) \times \{1 - \tanh[r/(\sqrt{2}\xi)]\}, \quad (1)$$

where σ_0 is the normalized ZBC away from a vortex core, r is the distance to the vortex center, and ξ is the GL coherence length in plane. The experimental data and fitted results for bare $NbSe_2$ and 3QL $Bi_2Te_3/NbSe_2$ are shown in Fig. 4(a), giving $\xi_{NbSe_2} = 16$ nm and $\xi_{5QL} = 29$ nm at 0.4 K and 0.1 T. Similar analyses were also performed on other samples, finding a monotonic increase of coherence length with Bi_2Te_3 thickness, as shown in Fig. 4(b). This is consistent with the above result that H_{c2} of 3QL $Bi_2Te_3/NbSe_2$ is smaller than that of bare $NbSe_2$, because

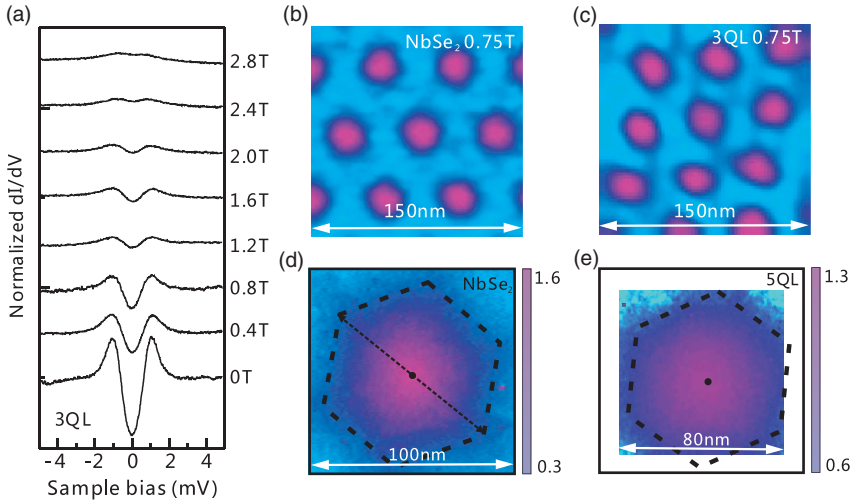

FIG. 3 (color). (a) Dependence of dI/dV spectra on the magnetic field, measured between vortices on a 3QL Bi_2Te_3 thin film at 0.4 K. (b) and (c) Zero-bias dI/dV maps measured at 0.4 K and 0.75 T for $NbSe_2$ and 3QL $Bi_2Te_3/NbSe_2$ heterostructures. (d) and (e) Zero-bias dI/dV maps for a single vortex measured at 0.4 K and 0.1 T on $NbSe_2$ and 5QL $Bi_2Te_3/NbSe_2$. The superimposed hexagons in dashed lines indicate the shape of the vortices. The profile along the dashed line through the center in (d) is fitted and shown in Fig. 4(a). The black dots at the center of vortex indicate the positions where the zero-bias conductance peaks [shown in Fig. 4(d)] are measured.

a larger ξ gives a smaller H_{c2} according the GL expression $H_{c2} = \Phi_0/(2\pi\xi^2)$.

Because the in-plane ξ of a $NbSe_2$ single crystal varies from 7.2 nm to 28.2 nm in previous reports [26,27], ξ obtained above for the bare $NbSe_2$ is a reasonable value. For epitaxial Bi_2Te_3 films, the superconducting coherence length should be estimated using its expression in the clean limit [23], $\xi_0 = hv_F/(\pi^2\Delta)$, in which v_F is the Fermi velocity, previously reported to be 3.32×10^5 m/s. This yields a ξ_0 value of 116 nm, much longer than that which has been seen experimentally. The discrepancy between the estimation and the above experimental results may be due to the difference between a proximity-induced and a pure superconductor. As the thickness of the Bi_2Te_3 film increases, the influence from the $NbSe_2$ substrate on the Bi_2Te_3 film becomes weaker, resulting in a longer coherence length.

Variation of the magnetic field leads to changes of the vortex size and the coherence length. The coherence length's dependence on the magnetic field is shown in Fig. 4(c) for 5QL $Bi_2Te_3/NbSe_2$. As the magnetic field increases, the coherence length decreases initially, and then saturates as the magnetic field reaches about 0.7 T. For a single-band s-wave superconductor, the vortex size or the coherence length is insensitive to the magnetic field at weak fields. The strong dependence of the vortex size with the field may be a characteristic feature of TSC. We note that the proximity-induced TSC on a d-wave superconductor has been reported recently [28].

The first step in detecting the topological superconductor is to observe the zero-bias conductance peak (ZBCP) caused by the bound states in the vortex core. The ZBCP was indeed observed in 1QL–6QL $Bi_2Te_3/NbSe_2$ at 0.1 T, as shown in Fig. 4(d). However, these peaks contain all of the bound states near the Fermi energy, and could not be identified as a signature of Majorana fermions. In fact, the peaks are also observed on bare $NbSe_2$ and 1QL–2QL Bi_2Te_3 films, and their heights are even higher than those of 3QL–6QL Bi_2Te_3 films. The bound states occur at energies where constructive interference forms from multiple reflected electronlike and holelike states. In a 2D chiral p-wave superconductor, the energy separation of the bound states is theoretically predicted to be $\delta E = \Delta_0^2/E_F$ [29], which is the minigap protecting the zero-energy Majorana fermion excitations from thermal effects. In recent theoretical work [30], the minigap of a proximity effect–induced TSC was found to be $\delta E \approx 0.83\Delta_0^2/\sqrt{\Delta_0^2 + E_F^2}$.

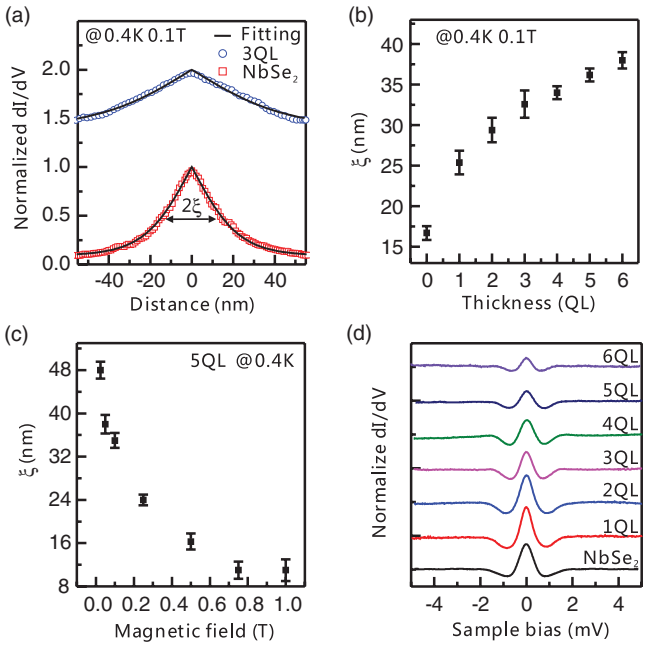

FIG. 4 (color). (a) Normalized ZBC profiles crossing through the centers of vortices at 0.4 K and 0.1 T on $NbSe_2$ and 3QL Bi_2Te_3, respectively. The superimposed lines are fitted results using Eq. (1). The 3QL data are shifted upward by 1.5 for a better view. The obtained coherence length as a function of thickness is summarized in (b). (c) The coherence length as a function of the magnetic field measured on 5QL $Bi_2Te_3/NbSe_2$. (d) Thickness dependence of dI/dV spectra measured at the centers of vortices on $NbSe_2$ and 1QL–6QL $Bi_2Te_3/NbSe_2$ at 0.4 K.

In order to increase the robustness of Majorana fermions to thermal effect, and to resolve them with STS, we need to decrease the sample temperature as much as possible and increase δE by shifting E_F towards the Dirac point. A 5QL $Bi_2Te_3/NbSe_2$ sample, for example, at a temperature of 300 mK corresponds to a thermal energy of 0.026 meV, if E_F can be shifted to within 5 meV of the Dirac point, the δE will be about 0.1 meV. This is much larger than the thermal energy, making the minigap detectable by STS. E_F can be tuned by doping, or alloying Sb_2Te_3 and Bi_2Te_3 [31]. However, chemical doping will reduce the sample quality. Experimental effort to achieve the precise control of E_F is highly desired.

In summary, we have provided experimental evidence for the superconductivity in TI surface states induced by the proximity effect. Abrikosov vortex lattices and bound states at the vortex cores were observed on proximity effect–induced TSC $Bi_2Te_3/NbSe_2$ heterostructures. Our study is a significant step in the search for Majorana fermions.

Jin-Peng Xu and Canhua Liu contributed equally to this Letter. This work was supported by the National Basic Research Program of China (Grants No. 2013CB921902, No. 2012CB927401, No. 2011CB921902, No. 2011CB922200, and No. 2012CB927403), NSFC (Grants No. 91021002, No. 11174199, No. 11134008, No. 11274228, No. 11274229, No. 11074043, and No. 11274269), Shanghai Committee of Science and Technology, China (Grants No. 11JC1405000, No. 11PJ1405200, and No. 12JC1405300), and Shanghai Municipal Education Commission (Grant No. 11ZZ17).

*Corresponding author.
jfjia@sjtu.edu.cn

[1] J. Kim, V. Chua, G. A. Fiete, H. Nam, A. H. Macdonald, and C. K. Shih, Nat. Phys. **8**, 464 (2012).
[2] J. Alicea, Rep. Prog. Phys. **75**, 076501 (2012).
[3] C. W. J. Beenakker, Annu. Rev. Condens. Matter Phys. **4**, 113 (2013).
[4] V. Mourik, K. Zuo, S. M. Frolov, S. R. Plissard, E. P. A. M. Bakkers, and L. P. Kouwenhoven, Science **336**, 1003 (2012).
[5] R. M. Lutchyn, J. D. Sau, and S. Das Sarma, Phys. Rev. Lett. **105**, 077001 (2010).
[6] M. Z. Hasan and C. L. Kane, Rev. Mod. Phys. **82**, 3045 (2010).
[7] D. Hsieh, D. Qian, L. Wray, Y. Xia, Y. S. Hor, R. J. Cava, and M. Z. Hasan, Nature (London) **452**, 970 (2008).
[8] L. Fu and C. L. Kane, Phys. Rev. Lett. **100**, 096407 (2008).
[9] J. R. Williams, A. J. Bestwick, P. Gallagher, S. S. Hong, Y. Cui, A. S. Bleich, J. G. Analytis, I. R. Fisher, and D. Goldhaber-Gordon, Phys. Rev. Lett. **109**, 056803 (2012).
[10] B. Sacepe, J. B. Oostinga, J. Li, A. Ubaldini, N. J. G. Couto, E. Giannini, and A. F. Morpurgo, Nat. Commun. **2**, 575 (2011).
[11] M. Veldhorst, M. Snelder, M. Hoek, T. Gang, V. K. Guduru, X. L. Wang, U. Zeitler, W. G. Van der wiel, A. A. Golubov, H. Hilgenkamp, and A. Brinkman, Nat. Mater. **11**, 417 (2012).
[12] F. M. Qu, F. Yang, J. Shen, Y. Ding, J. Chen, Z. Q. Ji, G. G. Liu, J. Fan, X. N. Jing, C. L. Yang, and L. Lu, Sci. Rep. **2**, 339 (2012).
[13] P. Zareapour, A. Hayat, S. Y. Zhao, M. Kreshchuk, A. Jain, D. C. Kwok, N. Lee, S. W. Cheong, Z. J. Xu, A. Yang, G. D. Gu, S. Jia, R. J. Cave, and K. S. Burch, Nat. Commun. **3**, 1056 (2012).
[14] I. Guillamón, H. Suderow, A. F. Pacheco, J. Sese, R. Cordoba, J. M. Teresa, M. R. Ibarra, and S. Vieira, Nat. Phys. **5**, 651 (2009).
[15] Ø. Fischer, M. Kugler, I. M. Aprile, and C. Berthod, Rev. Mod. Phys. **79**, 353 (2007).
[16] M. R. Eskildsen, M. Kugler, S. Tanaka, J. Jun, S. M. Kazakov, J. Karpinski, and Ø. Fischer, Phys. Rev. Lett. **89**, 187003 (2002).
[17] M. X. Wang, C. H. Liu, J. P. Xu, F. Yang, L. Miao, M. Y. Yao, C. L. Gao, C. Y. Shen, X. C. Ma, Z. A. Xu, Y. Liu, S. C. Zhang, D. Qian, J. F. Jia, and Q. K. Xue, Science **336**, 52 (2012).
[18] X. Chen, X. C. Ma, K. He, J. F. Jia, and Q. K. Xue, Adv. Mater. **23**, 1162 (2011).
[19] Y. Y. Li, G. Wang, X. G. Zhu, M. H. Liu, C. Ye, X. Chen, Y. Y. Wang, K. He, L. L. Wang, X. C. Ma, H. J. Zhang, X. Dai, Z. Fang, X. C. Xie, Y. Liu, X. L. Qi, J. F. Jia, S. C. Zhang, and Q. K. Xue, Adv. Mater. **22**, 4002 (2010).
[20] K. Park, J. J. Heremans, V. W. Scarola, and D. Minic, Phys. Rev. Lett. **105**, 186801 (2010).
[21] Y. Liu, G. Bian, T. Miller, M. Bissen, and T. C. Chiang, Phys. Rev. B **85**, 195442 (2012).
[22] A. M. Black-Schaffer and A. V. Balatsky, Phys. Rev. B **87**, 220506(R) (2013).
[23] G. Tkachov, Phys. Rev. B **87**, 245422 (2013).
[24] R. C. Dynes, V. Narayanamurti, and J. P. Garno, Phys. Rev. Lett. **41**, 1509 (1978).
[25] H. F. Hess, R. B. Robinson, R. C. Dynes, J. M. Valles, Jr., and J. V. Waszczak, Phys. Rev. Lett. **62**, 214 (1989).
[26] J. E. Sonier, R. F. Kiefl, J. H. Brewer, J. Chakhalian, S. R. Dunsiger, W. A. MacFarlane, R. I. Miller, A. Wong, G. M. Luke, and J. W. Brill, Phys. Rev. Lett. **79**, 1742 (1997).
[27] R. I. Miller, R. E. Kiefl, J. H. Brewer, J. Chakhalian, S. Dunsiger, G. D. Morris, J. E. Sonier, and W. A. MacFarlane, Phys. Rev. Lett. **85**, 1540 (2000).
[28] E. Wang, H. Ding, A. V. Fedorov, W. Yao, Z. Li, Y. F. Lv, K. Zhao, L. G. Zhang, Z. J. Xu, J. Schneeloch, R. Zhong, S. H. Ji, L. L. Wang, K. He, X. C. Ma, G. Gu, H. Yao, Q. K. Xue, X. Chen, and S. Y. Zhou, Nat. Phys. **9**, 621 (2013).
[29] C. Caroli, P. G. De Gennes, and J. Matricon, Phys. Lett. **9**, 307 (1964).
[30] J. D. Sau, R. M. Lutchyn, S. Tewari, and S. Das Sarma, Phys. Rev. B **82**, 094522 (2010).
[31] J. Zhang, C. Z. Chang, Z. Zhang, J. Wen, X. Feng, K. Li, M. Liu, K. He, L. Wang, X. Chen, Q. K. Xue, X. C. Ma, and Y. Y. Wang, Nat. Commun. **2**, 574 (2011).